SUPPLEMENTARY INFORMATION

Shelf hypoxia in response to global warming after the Cretaceous-Paleogene boundary impact

Johan Vellekoop[1,2 *], Lineke Woelders[1], Niels A.G.M. van Helmond[3], Simone Galeotti[4], Jan Smit[5], Caroline P. Slomp[3], Henk Brinkhuis[6], Philippe Claeys[2], Robert P. Speijer[1]

AFFILIATIONS

[1]Department of Earth and Environmental Sciences, KU Leuven University, Celestijnenlaan 200E, 3001 Heverlee, Belgium.

[2]AMGC, Vrije Universiteit Brussel, Pleinlaan 2, B-1050, Brussels, Belgium.

[3]Department of Earth Sciences, Faculty of Geosciences, Utrecht University, PO Box 80021, 3508 TA Utrecht, The Netherlands.

[4]Department of Earth, Life and Environmental Sciences, University of Urbino 'Carlo Bo', Loc Crocicchia s.n., 61029 Urbino, Italy.

[5]Department of Sedimentology and Marine Geology, VU University Amsterdam, de Boelelaan 1085, 1018HV Amsterdam, The Netherlands.

*e-mail: johan.vellekoop@ kuleuven.be

Supplementary Materials, Methods and Estimations

Materials

1.1 Brazos-1 (USA)

1.1.1 Geological setting

1.1.2 Sampling

1.1.3 Age Model

1.2 Stevns Klint (Denmark)

1.2.1 Geological setting

1.2.2 Sampling

1.2.3 Age Model

1.3 Caravaca (Spain)

1.3.1 Geological setting

1.3.2 Sampling

1.3.3 Age Model

Methods

2.1 Reconstruction oceanic anoxia in the geological past

2.2 hexaperidinioids as indicator for nutrients or fresh water

Estimations

3.1 Estimations of CO_2 release by Chicxulub impact

SI Materials and Methods

1 Materials

1.1 Brazos–1

1.1.1 Geological setting

During the Late Cretaceous and early Paleogene, the Brazos area was situated on the northern shelf of the Gulf of Mexico (Kennedy et al., 1998), with estimated water depths of 75–100 m (Smit et al., 1996; Woelders and Speijer, 2015) and a paleolatitude of approximately 35N (Scotese and Dreher, 2012). The sedimentary successions in this region comprise the Maastrichtian Corsicana Formation and the Paleocene basal and upper Littig members of the Kincaid Formation. The K-Pg boundary deposits outcropping along the Brazos River between Waco and Hearne, Texas, comprise an exceptionally well-preserved and frequently studied sedimentary succession (Smit et al., 1996; Woelders and Speijer, 2015; Hansen et al., 1987; Bourgeois et al., 1988; Yancey, 1996; Heymann et al., 1998; Vellekoop et al., 2014;

Ganapathy et al., 1981). In most previous studies, the K-Pg boundary interval has been subdivided in a series of lithological units (Units A to J) first described by Hansen et al. (1987). The uppermost Maastrichtian Corsicana Formation consists of dark grey–brown mudstones, which include occasional shell hashes and small molluscs. The superimposed Lower Littig Member consists of a distinct sequence of graded shell-hashes, cross-bedded sands and silts that is sometimes referred to as the K-Pg boundary "sandstone complex" (Units B-G) (Smit et al., 1996). The "sandstone complex" is further subdivided into a lower (B-D) and an upper complex (E-G). The lower complex has been interpreted as tsunami deposits triggered by the Chicxulub impact on the Yucatan peninsula, present day Mexico (Smit et al., 1996; Hansen et al., 1987; Bourgeois et al., 1988; Yancey, 1996; Hildebrand et al., 1991). Abundant altered impact spherules have been found in the lower B/C units (Smit et al., 1996), mixed in with backwashed local seafloor debris such as shell hash, fish-teeth, glauconite pellets and shallow-water foraminifera. Unit D consists of cross-bedded medium to fine-grained sands, displaying mainly climbing-ripple tracts from the tsunami backwash. The sequence C-E may repeat locally up to four times, reflecting backwash from several individual tsunami surges. The upper complex of the K-Pg boundary "sandstone complex" comprises Units E, F and G, grading from very fine sand, to silt to mudstone. The base of this complex consists of a 1-2 cm thick siltstone (Unit E), overlain by a silty limestone (Unit F, 8 cm thick), and a subsequent grey claystone (Unit G, 10 cm). This complex shows a normal gradation and has been interpreted to be deposited within a time span of 24 hours to a couple of weeks, as part of the settling phase of the tsunami complex deposited directly after the K-Pg boundary bolide impact in the Gulf (Smit et al., 1996). However, the iridium records already show elevated levels at the base of Unit E (Ganapathy et al., 1981; Hansen et al., 1987; Asaro et al., 1982; Rocchia et al., 1996). Since it may take days to years to deposit the very fine-grained impact-derived Platinum Group Elements (PGEs) on the sea floor (Robin et

al., 1991; Kring and Durda, 2002), longer than the dissipation of the impact-triggered tsunami waves, the complex of Units E-G probably represents a rapid depositional event that occurred at least weeks *after* the K-Pg boundary tsunamis, possibly as the deposition of suspended material after the waning of large storms and hurricanes that occurred in the decades following the K-Pg boundary impact (Vellekoop et al., 2014; Hart et al., 2012). Moreover, according to the study of (Hart et al., 2012), the *entire* K-Pg boundary sandstone complex at Brazos River represents storm lag deposits, deposited on top of the tsunami-scoured surface. At least the PGE-bearing, immediate post-impact sediments have probably been rapidly redeposited in the upper complex of Units E-G by these storms (Vellekoop et al., 2014). For a more detailed discussion on the origin of the complex of lithological units E-G, see (Hart et al., 2012) and (Vellekoop et al., 2014). This complex of units E-G is overlain by a <5 cm thick, laminated sandy bed with small shells and thin clay flakes (Unit H), which may represent the last lag deposit resulting from a large storm passing this site. Following this is Unit I, a ~2.5 m thick silty claystone that is herein interpreted as representing the resumption of normal marine shelf sedimentation at this site. This unit is unconformably overlain by the lag deposit of the Kincaid Formation, the upper Littig Member (Unit J). This member is composed of a 0.3-0.6 meter thick glauconitic sandy clay with grains, granules and pebbles.

1.1.2 Sampling

At Brazos River, the Paleocene stratigraphy varies considerably between individual outcrops and cores (e.g. (Hart et al., 2012)), so first and last appearances and amount of reworking are difficult to compare between the various sequences. The Brazos-1 outcrop (BR1), the first well-studied outcrop, has been partially destroyed due to sampling excavations and is currently inaccessible because of recent fluvial activity, which renders additional sampling impossible. To allow for a precise correlation with the biostratigraphic and organic geochemical

analyses of (Vellekoop et al., 2014), our analyses on organic-walled dinoflagellate cysts, benthic foraminifera and trace elemental compositions were all performed on the same sample set (acquired in 1995 by JS from the Brazos-1 outcrop; GPS 31° 7′53.59″N, 96°49′26.08″W), when the outcrop was still relatively well exposed and accessible. In the extensive 1995 sampling performed at BR1, care was taken to acquire non-weathered rock samples, to obtain well-preserved microfossils and limit possible contamination. A closely spaced sample set was obtained, to attain a high temporal resolution. The stratigraphic position was measured from the base of the graded silty limestone, Unit F, since this level is sharp, well visible and constant throughout the outcrops in the Brazos area. In total, about 100 samples were collected between 500 cm below the base of Unit F and 420 cm above the base of Unit F. The beds directly above the top of the sandstone (interval E-H) were sampled in large continuous blocks, which were slabbed into slices of 0.5 cm thickness. Unit I was sampled at 5 cm spacing in the first 2.5 m above the sandstone beds, the remainder up to the Littig bed at 10 cm and the top of the section at 25 cm intervals. The samples were split in aliquots for analyses of planktic and benthic foraminifers, organic-walled dinoflagellate cysts, TEX_{86} and trace-elements. All samples were oven-dried at 60°C and stored at the VU University Amsterdam Faculty of Earth and Life Sciences sample storage, the Netherlands. A selection of these samples was used in the present study.

1.1.3 Age Model

The high-resolution age model used in this study is based on the Ir-anomaly and calcareous nannoplankton, planktic foraminifer and organic-walled dinoflagellate cyst (dinocyst) biostratigraphy presented in (Vellekoop et al., 2014). Various studies have been published on iridium anomalies in the Brazos River area (Ganapathy et al., 1981; Asaro et al., 1982; Rocchia et al., 1996; Hansen et al., 1993), showing a series of irregular peaks in lithological Units E, F and G. It is likely that the PGE bearing impact dust settled within months to years after the

impact and was subsequently reworked in the lag deposits of post-impact storms (Vellekoop et al., 2014; Hart et al., 2012), explaining the scattered and smeared out nature of the iridium profile. Since the enhanced contrast between warm oceans and cold atmosphere, triggering the storms after the impact, likely lasted for less than a century (Vellekoop et al., 2014; Galeotti et al., 2004), we assume that this is the maximum amount of time represented by units E, F and G. Normal sedimentation resumed in Unit I, which therefore represents the first millennia following the K-Pg boundary impact winter event. The impact winter event is suggested to have had a duration of 1-30 years (Galeotti et al., 2004; Vellekoop et al., 2014; Brugger et al., 2016)

(Jiang and Gartner, 1986) published detailed, semi-quantitative nannofossil data from a closely spaced sample set from the Brazos-1 locality. (Vellekoop et al., 2014) argued that their results could be tied in with the earlier published biostratigraphic data from (Jiang and Gartner, 1986), because their samples were derived from the same outcrop. In the nannofossil record of (Jiang and Gartner, 1986) the earliest Paleocene Kincaid Formation contains a rapid succession of basal Paleocene assemblages. The basal meter of the Kincaid Fm. above the "sandstone complex" is dominated by inferred disaster taxa, such as species of the calcareous dinoflagellate cyst *Thoracosphaera* and the calcareous nannoplankton species *Braarudosphaera bigelowii*. Blooms of *Thoracosphaera* have been recorded in the earliest Paleocene at many different sites (Lottaroli and Catrullo, 2000; Gardin, 2002) and are considered a characteristic feature for the lowermost Danian.

The foraminiferal biozonation applied in this paper follows that of (Olsson et al., 1999) and is based on the biostratigraphic datum events of Vellekoop et al. (2014). The Maastrichtian samples contain well-preserved, moderately abundant Maastrichtian planktic foraminiferal assemblages. The first Paleocene taxon, *Parvulorugoglobigerina minutula*, appears in Br95-23, followed by the lowest occurrence of *Parvulorugoglobigerina alabamensis* [in sample Br95-24]. *Chiloguembelina* sp. and *Woodringina* sp. appear in sample Br95-30. These taxa are

initially very rare and do not show up in the counts of 300 random selected specimens. *Parvulorugoglobigerina eugubina* appears in sample Br95-26 (~150 cm above the K-Pg boundary). This sequence of lowest occurrences of *P. minutula*, *P. alabamensis* and *P. eugubina* is very similar to the expanded lowermost Paleocene section of the K-Pg boundary global stratotype and section at El Kef in Tunisia (Smit, 1982).

When the tsunami- and storm-induced graded beds (Units A-H), with a combined thickness of 50 cm, are disregarded, biozone P0 attains a thickness of around 100 cm in Brazos-1, based on the lowest occurrence of *P. eugubina*. This interval is entirely characterized by background middle-to-outer shelf mudstones (Unit I), with no sandstones. It is therefore reasonable to assume that sedimentation rates are fairly constant throughout Zone P0. According to the Paleogene time scale of (Vandenberghe et al., 2012), based on the study of (Wade et al., 2011), planktic foraminiferal Zone P0 represents approximately 30-40 kyrs, resulting in an average sedimentation rate of ~2.5-3 cm/kyr for the lowermost Danian of Brazos-1. The onset of the warming in the TEX_{86} SST record of (Vellekoop et al., 2014), which covers an interval of approximately 15 cm, therefore represents the first 4-6 kyrs of the Paleocene, assuming constant background sedimentation. The total warming event covers an interval of more than 75 cm at Brazos-1, representing at least ~30 kyrs.

1.2 Stevns Klint

1.2.1 Geological setting

The Stevns Klint succession is one of the first localities where the base of the Danian was defined (Desor, 1847). Since then, numerous paleontological, geochemical and mineralogical studies have been performed on this succession (e.g. (Hansen, 1977; Bauluz et al., 2000; Hart et al., 2004; Rasmussen et al., 2005; Premovic, 2009; Hansen and Surlyk, 2014). The 14.5 km long coastal cliff is situated about 45 km south of Copenhagen, on the east coast of the Danish

188 Island of Zealand. The upper Maastrichtian-lower Danian succession exposed at Stevns Klint
189 was deposited on the eastern edge of the Ringkøbing-Fyn structural high, which forms the
190 southern border of the Danish Basin. The chalk and bryozoan limestones of Stevns Klint were
191 thus deposited in shallower-water than the correlative deposits of the Danish Basin and the
192 North Sea (references in (Surlyk et al., 2006)). The Stevns Klint K-Pg boundary succession is
193 estimated to be deposited at depths of about 100–150 m (Bromley and Ekdale, 1987), at a
194 paleolatitude of approximately 46N (Scotese and Dreher, 2012).

195 The succession studied here consists of the Maastrichtian Tor Formation and Danian
196 Rodvig Formation. The lower part of the Maastrichtian Tor Formation consists of the mound-
197 bedded chalk of the Sigerslev Member. This member is topped by two closely spaced incipient
198 hardgrounds, characterized by nodular hardening and an irregular, small-scale erosional relief
199 of a few centimeters. The distance between the two incipient hardgrounds is generally 10-25
200 cm. Occasionally, these incipient hardgrounds may merge into a single hardground. A
201 prominent layer of nodular flint occurs 30-50 cm below the upper hardground and forms a
202 marker bed, which can be traced along most of the cliff.

203 The overlying Hojerup Member of the Tor Formation consists of mounded bryozoan chalk
204 wackestone. This unit, previously labelled as “Grey Chalk”, is up to 5 m thick but gradually
205 wedges out towards the north of the cliff, possibly due to reduced sedimentation. The top few
206 centimeters of the Hojerup Member are developed as grey marl.

207 The Hojerup Member is overlain by the basal Danian Fiskeler Member of the Rodvig
208 Formation. The boundary between the Hojerup Member and the Fiskeler Member is sharp and
209 represents the Cretaceous-Paleogene boundary. The Fiskeler Member embodies a classical
210 ‘boundary clay layer’. The Fiskeler clay is restricted to the depressions between the crests of
211 the Hojerup Member mounds and thins towards the margins of these depressions. At the crests

of the Hojerup Member mounds, the hardened Maastrichtian chalk wackestone is directly overlain by the lower Danian *Cerithium* Limestone Member. Although the Fiskeler Member is up to about 10 cm thick in most of the cliff, it shows thicknesses up to 30 cm to the north at Kulstirenden. In this study, the samples were taken at Kulstirenden. At this site, the base of the Fiskeler Member is characterized by a 0.1-0.5 cm thick, reddish (iron-oxide stained) layer that represents the global ejecta layer, comprising the classical markers for the K-Pg boundary, e.g. microkrystites, the iridium anomaly and other geochemical markers (Alvarez et al., 1980; Bauluz et al., 2000). A 4-5 cm thick black (weathering brown) clay bed with pyrite concretions overlies this reddish layer. This clay bed ("bed a" by Surlyk et al. (Surlyk et al., 2006)) is characterized by pale/dark alternations near the top. In turn, it is overlain by a 14-15 cm thick black to light grey streaky marl ("bed b" in (Surlyk et al., 2006)). This bed is restricted to the deepest parts of the depressions between the bryozoan mounds. There is no sign of bioturbation within beds a and b, which suggests that the sea floor environment would have been (almost) anoxic (Hart et al., 2005). This bed is again overlain by a light-grey streaked marl, up to 7 cm thick – "bed c" of Surlyk et al. (Surlyk et al., 2006). Bed c can be followed to the margins of the depressions. The Fiskeler Member becomes more carbonate-rich upwards and passes gradually into the *Cerithium* Limestone Member.

The *Cerithium* Limestone Member consists of micrite and is strongly burrowed by *Thalassinoides*. These burrows are filled with sediment derived from the overlying lower Danian bryozoan limestone. The base of the *Cerithium* Limestone Member contains abundant clasts of chalk, probably derived from erosion of the crests of the Maastrichtian bryozoan mounds (Surlyk et al., 2006).

An erosional surface truncates the top of the *Cerithium* Limestone Member and the crests of the bryozoan mounds of the uppermost Maastrichtian Hojerup Member. At Kulstirenden it is

developed as a double hardground, similar to the one at the base of the Hojerup Member. The upper 35 cm of sediment beneath the upper hardground surface is strongly cemented.

1.2.2 Sampling

For this study, a fieldwork to the cliffs of Stevns Klint, Denmark was organized in the summer of 2016. Given that the Fiskeler Member reaches its maximum thickness at Kulstirenden (25-30 cm), this site provides the highest possible stratigraphic resolution. Therefore, in our study, samples were taken at this site (GPS 55°20′45.84″N, 12°26′43.21″E).

Since the uppermost Cretaceous Hojerup Member gradually wedges out towards the north, it is rather thin at Kulstirenden. At the base of the basins between the bryozoan mounds, the Hojerup Member is condensed to single, nodular, silicified layer, merged with the hardgrounds that form the top of the Sigerslev Member. To allow for relative high temporal resolution in both the Cretaceous and Paleogene, the Fiskeler Member was sampled in one of the basins between the Hojerup Member bryozoan mound crests, where the Fiskeler K-Pg boundary clay reaches a thickness of 27-28 cm (Kulstirenden A), while the Sigerslev and Hojerup Members were sampled about 15 meters lateral from this point (Kulstirenden B), where the Hojerup Member reaches a thickness of approximately 1 meter see SI Figure S1). Our record from Kulstirenden, Stevns Klint, is a composite of these 2 sample sets.

The Sigerslev Member was sampled at 50 cm resolution, the Hojerup Member was sampled at 5 cm resolution, the Fiskeler Member was sampled with a 1 cm resolution.

1.2.3 Age Model

At Stevns Klint, the K-Pg boundary is characterized by the classical markers for the K-Pg boundary impact, such as the Ir-anomaly (Alvarez et al., 1980), micrometeorites (Korchagin and Tsel'movich, 2011) and impact glass (Bauluz et al., 2000). The high-resolution age model used in this study is based on these markers, in combination with planktic foraminiferal and organic-walled dinoflagellate cyst (dinocyst) biostratigraphy, e.g. (Hansen, 1977; Brinkhuis et al., 1998; Rasmussen et al., 2005). The foraminiferal biozonation applied in this paper follows that of Olsson *et al.* (Olsson et al., 1999) and is based on (Rasmussen et al., 2005; Schmitz et al., 1992).

(Rasmussen et al., 2005) argued that the Fiskeler Member corresponds to the lowermost Paleocene planktic foraminiferal Zone P0. The dinoflagellate studies of (Brinkhuis et al., 1998) and (FitzPatrick et al., 2017) demonstrated that the Fiskeler Member is characterized by the first occurrences of the marker taxa *Senoniasphaera inornata* and *Carpatella cf. cornuta*, similar to the boundary clay layer of the K-Pg boundary GSSP at El Kef (Tunisia), comfirming the assignment of Zone P0 to the Fiskeler Member

When the Fiskeler Member is considered as representing planktic foraminiferal Zone P0 of (Olsson et al., 1999), this biozone attains a thickness of around 27-28 cm at the Kulstirenden A outcrop of Stevns Klint. As planktic foraminiferal Zone P0 represents approximately 30-40 kyrs (Vandenberghe et al., 2012), the Fiskeler Member at Kulstirenden has an average sedimentation rate of ~0.7-1.0 cm/kyr. While it is possible that sedimentation rates might have varied trough the boundary clay layer, this will likely not have been in orders of magnitude, as the resumption of carbonate production occurs above the boundary clay layer. It is therefore reasonable to assume that the first few centimeters of the boundary clay layer represent the first millennia after the K-Pg boundary impact.

1.3 Caravaca

1.3.1 Geological setting

The Caravaca section is located about 4 km southwest of the town of Caravaca (Murcia, Spain), in the Betic Cordillera. The sequence of the Jorquera Formation, which encompasses the K-Pg boundary, is exposed on the east bank of the Barranco del Gredero.

The lithology of this succession consists of uppermost Maastrichtian light marls, followed by a 7–10 cm lower Danian (lowermost Paleocene) dark grey clay layer, the K-Pg boundary clay layer. The 2–3 mm thick reddish brown (ejecta) layer) at the base of the boundary clay contains microspherules and platinum group element (PGE) anomalies (e.g. (Smit, 1990, 2004; Martinez-Ruiz et al., 2006)). Between 5 and 10 cm, the boundary clay gradually grades into a grey argillaceous marl, similar to that of the upper Maastrichtian (Figure 1). The Caravaca section, like the nearby Agost section (at 115 km distance in southeastern Spain) and the El Kef section (Tunisia), is one of the best-preserved distal K-Pg boundary sections in the world (Molina et al., 2006). The Caravaca succession is estimated to have been deposited at a paleodepth of 500-1000 m (Smit, 2004; Culver, 2003), and its paleolatitude was approximately at 27N (Scotese and Dreher, 2012).

For a detailed description of the Caravaca section, see the study of (Smit, 2004).

1.3.2 Sampling

For this study, the extensive sample set of (Smit, 1977) was used. This set, taken in 1975, has a 1-cm resolution through the boundary clay, approaching the sample resolution of the benthic foraminiferal study of (Coccioni and Galeotti, 1994), with which we compare our results.

1.3.3 Age Model

At Caravaca, the K-Pg boundary is characterized by the classical impact markers (microspherules and PGE anomalies (e.g. (Smit, 1990, 2004; Martinez-Ruiz et al., 2006))). The high-resolution age model used in this study is based on these markers, in combination with calcareous nannofossil, planktic foraminiferal and organic-walled dinoflagellate cyst (dinocyst) biostratigraphy, e.g. (Coccioni and Galeotti, 1994; Brinkhuis et al., 1998; Smit, 2004). The foraminiferal biozonation applied in this paper follows that of (Olsson et al., 1999) and is based on the data of (Smit, 1982). The dinoflagellate study of (Brinkhuis et al., 1998) demonstrated that the boundary clay at Caravaca is characterized by the first occurrences of the marker taxa *Senoniasphaera inornata* and *Damassidinium californicum*, similar to the boundary clay at the Danian GSSP of El Kef (Tunisia).

At Caravaca, planktic foraminiferal Zone P0 attains a thickness of 7-10 cm, approximately corresponding with 30-40 kyrs (24, 25), resulting in an average sedimentation rate of ~0.2-0.3 cm/kyr.

2 Methods

2.1 Reconstruction of oceanic anoxia in the geological past

A wide range of proxies can be employed for the reconstruction of redox conditions. A simple proxy is the total organic carbon content (TOC) of sediments. However, along with bottom-water oxygen conditions, TOC content is also a function of the organic matter flux to the seafloor. Given that the K-Pg boundary is characterized by strong changes in the transport of organic matter to the sea floor (e.g. (Vellekoop et al., 2017), this proxy is not well-suited to reconstruct changes in bottom-water oxygenation across this time interval. Concentrations of trace metals in sediments, e.g., V, Cr, Cu, Zn, Ni and in particular Mo, have been shown to be

329 excellent proxies for paleo-redox conditions in bottom waters (Brumsack, 1980; Emerson and
330 Huested, 1991; Scott and Lyons, 2012), as was also illustrated for the K-Pg boundary (Sosa-
331 Montes De Oca et al., 2013; Kaiho et al., 1999). These elements are actively scavenged from
332 oxygen-depleted marine environments, and therefore enriched in the sediments. Under
333 euxinic conditions, molybdate anions are converted to particle-reactive thiomolybdates, hence
334 allowing for burial of Mo in the sediments (Helz et al., 1996). Therefore, enrichments of
335 elementary Mo can be used as an indicator for sea floor deoxygenation (Thomson et al., 1995;
336 Scott and Lyons, 2012).

337 For the analyses of major and minor element compositions, approximately 125 mg of
338 freeze-dried and powdered sample was dissolved in 2.5 ml mixed acid ($HClO_4$;HNO_3; 3:2)
339 and 2.5 ml 40% HF, heated to 90°C and left overnight. The acids were evaporated at 140°C
340 after which the residue was dissolved in 25 ml 4.5% HNO_3. Sediment elemental compositions
341 were measured using Inductively Coupled Plasma-Optical Emission Spectrometry (ICP-OES;
342 Perkin Elmer Optima 3000); the error calculated from duplos and standards generally was
343 <1ppm for Mo. Concentrations of measured elements Al and Mo can be found in
344 Supplementary Table S1.

345 Benthic foraminiferal assemblages can be excellent indicators for the biotic responses
346 to changes in bottom water oxygenation (Jorissen et al., 2007, 1995). For benthic
347 foraminiferal analysis, 79 samples were weighed and washed over a nylon mesh of 63µm. A
348 suitable split with approximately 200-400 specimens was obtained from the fraction greater
349 than 63µm with a microsplitter. From this split all the specimens were picked, counted and
350 mounted on micropaleontological slides (Supplementary Table S2). Samples from Unit G and
351 Unit H of Brazos-1 did not provide more than 50-60 specimens, however. Taxonomy used
352 follows that cited in (Woelders and Speijer, 2015).

Specific taxa are considered indicative of dysoxic to anoxic conditions and the relative frequency of these taxa (expressed as a percentage of the total benthic foraminiferal fauna) is used as a semi-quantitative index of bottom water oxygenation (Jorissen et al., 2007). A strong dominance of endobenthic taxa is typically considered indicative for bottom-water dysoxia to anoxia, often under eutrophic conditions (Jorissen et al., 2007). In the Brazos-1 record, the initial peak of the endobenthic foraminifera is almost entirely represented by the genus *Fursenkoina* (SI Figure S2). In sub-recent to recent settings, *Fursenkoina* is considered tolerant to low oxygen conditions (Kaiho, 1994).

2.2 Hexaperidinioids as indicator for nutrients or fresh water

For palynological analyses, 84 oven-dried samples (~10-15 g dry mass) were analyzed. Chemical processing comprised treatment with 10% HCl and 40% HF for carbonate and silica removal, respectively. Ultrasonication was used to disintegrate palynodebris. Residues were sieved over a 15-µm mesh and mounted on microscope slides, which were analyzed at x200 and x1000 magnification to a minimum of 200 dinocysts (Supplementary Table S3). Taxonomy used follows that of Vellekoop *et al.* (Vellekoop et al., 2014). All slides are stored in the collection of the Laboratory of Palaeobotany and Palynology, Utrecht University, the Netherlands.

Based on correlations between palynological records and other paleoproxies, it has been suggested that hexaperidinioids are indicative of high nutrient availability and/or low salinities (Eshet et al., 1994; Brinkhuis et al., 1998; Sluijs and Brinkhuis, 2009). Therefore, high abundances of this morphological group can be related to changes in trophic condition as well as to changes in salinity. The Brazos-1 and Stevns Klint sequences are deposited in neritic settings. Therefore, changes in both salinity and nutrient loading can be expected. To assess the

possibility that the signals in the palynological record can be attributed to changes in freshwater input, we tested for a significant correlation between relative abundances of hexaperidinioids and relative abundances of terrestrial palynomorphs in the Brazos-1 and Stevns Klint datasets, following Vellekoop et al. (Vellekoop et al., 2017). Pollen and spores are land-derived and can therefore be regarded as a proxy for the input of terrestrial-derived material. Since a hypothetical decrease in salinity would most likely be associated with increased riverine input, the input of terrestrial-derived material is expected to increase with decreasing salinity.

Our analyses show that in the Brazos-1 dataset, there is a significant relationship between the relative abundances of hexaperidinioids and the relative abundances of terrestrial palynomorphs, $r(84) = 0.32705$, $p < 0.05$ (SI Figure S3), but that there is a large variability in hexaperidinioids, that can only partly be explained by relative abundances in terrestrial palynomorphs. Therefore, at Brazos-1, high abundances of hexaperidinioids are considered in part indicative of increased freshwater input, but they likely also require other factors, such as high nutrient availability in the upper water column. In the Stevns Klint dataset, there is no significant relationship between the relative abundances of hexaperidinioids and the relative abundance of terrestrial palynomorps, $r(15) = 0.253403$, $p > 0.05$ (SI Figure S3). Therefore, at Stevns Klint, high abundances of hexaperidinioids are likely related to high nutrient availability in the upper water column, not directly to increased freshwater input.

3 Estimations

3.1 Estimations of CO_2 release by Chicxulub impact

Estimations of the amount of CO_2 released from the targeted carbonate platform greatly depend on the assumed thickness of the carbonate platform (O'Keefe and Ahrens, 1989), pressure generated by the impact (Ivanov and Deutsch, 2002) and exact chemical

composition of the shock-induced gases (Kawaragi et al., 2009). The estimated amount of CO_2 therefore ranges between 425 and 10,000 Gt (O'Keefe and Ahrens, 1989; Kawaragi et al., 2009; Ivanov et al., 1996; Pierazzo et al., 1998; Pope et al., 1997; Takata and Ahrens, 1994; Artemieva and Morgan, 2017).

In addition to the CO_2 released from the targeted carbonates, a large quantity of CO_2 must have been released by the combustion following the impact (Venkatesan and Dahl, 1989; Anders et al., 1990; Harvey et al., 2008). This combustion event possibly involved the global ignition of forest fires, resulting from the intense heat pulse from the impact (Anders et al., 1990). In the modern day, roughly 600 Gt C is stored in terrestrial vegetation (e.g. ref. (Potter et al., 1999), representing ~2200 Gt CO_2). In the Maastrichtian, vegetation cover was likely similar to, or larger than, at present (Hunter et al., 2008; Vajda and Bercovici, 2014), suggesting that the amount of carbon stored in terrestrial biomass was *at least* of a similar order. Although evidence for wildfires at the K-Pg boundary is widespread (e.g. USA; New Zealand; Japan; e.g. ref. (Vajda et al., 2001)), it is not realistic that the global vegetation was entirely combusted at the impact. The amount of CO_2 produced will nonetheless have been significant (~250-1000 Gt?; (Venkatesan and Dahl, 1989)). The impact may have also combusted a significant part of the surrounding organic-rich deposits (Harvey et al., 2008; Kaiho and Oshima, 2017). Indeed, the signature of pyrosynthetic polycyclic hydrocarbons (pPAHs) in the K-Pg boundary impact layer is consistent with the combustion of a large volume of hydrocarbons (Belcher et al., 2009). The carbon released by the impact-triggered combustion of subsurface hydrocarbons likely represents at least another >500 Gt of CO_2 (Harvey et al., 2008). Combined, the estimated amount of CO_2 released by the K-Pg impact ranges between ~1500 and ~10,000 Gt of CO_2.

Besides this direct release of CO_2 by the impact, the loss of the oceanic biological pump (Hondt, 2005; Vellekoop et al., 2017) reduced the ability of the world oceans to

efficiently deliver CO_2 to the deep ocean. When the biological pump is operating at lowered efficiency, surface water CO_2 concentrations tend to increase (Sarmiento et al., 2004; Hilting et al., 2008). The reduction of the biological pump likely led to increased remineralisation of organic matter in the surface waters (Vellekoop et al., 2017) and ventilation of CO_2 to the atmosphere and therefore to an additional rise in atmospheric pCO_2. Although the exact amount of CO_2 released to the atmosphere greatly depends on factors such as the rate of ocean circulation and the drawdown of CO_2 by surviving phytoplankton groups, it likely represented a considerable amount. (Beerling et al., 2002) estimated the rise in pCO_2 related to this process to be in the order of 400-800 ppm, although this might be an overestimation, as the biological drawdown did not come to a complete halt (Alegret and Thomas, 2009).

3.2 Estimations of increase atmospheric pCO_2 resulting from the impact

Studies using fossil leaf stomatal abundances and paleosol proxies suggest that latest Maastrichtian atmospheric CO_2 levels roughly ranged between 400-800 ppmv (Beerling et al., 2002; Royer et al., 2012), about 1.5 to 3 times pre-industrial levels. With a total of between 1500 and 10,000 Gt CO_2 released by the K-Pg boundary impact directly, the increase of atmospheric pCO_2 will have been in the order of ~200-1200 ppmv. With the additional input of CO_2 resulting from the collapse of the biological pump, the increased in atmospheric pCO_2 likely was in the order of 1-2 times the pre-impact level. Although this estimated increase is less then estimated based on fossil leaf stomatal indices (>2000 ppm; ref. (Beerling et al., 2002); representing a 2-5 times increase), this input still represents a large and near-instantaneous increase in atmospheric pCO_2 concentration, resulting in a rapid global warming in the first centuries following the brief K-Pg boundary impact winter.

Global records of shelf hypoxia

4.1. Global records of shelf hypoxia

In the past decades, several other studies have argued for short-lived shelf hypoxia following the Chicxulub impact as well. In most cases, this postulation is based on abrupt changes in benthic foraminiferal assemblages. Records from shelf sites such as El Kef (Tunisia), Agost (Spain), Caravaca (Spain) and Bidart (France) show a spike in endobenthic morphotypes in the lowermost centimeter(s) of the boundary clay (Speijer and Zwaan, 1996; Kaiho et al., 1999; Coccioni and Galeotti, 1994; Alegret et al., 2003), or inside post-K-Pg trace fossils hosted in uppermost Cretaceous strata (Alegret et al., 2015). Often, this spike is dominated by bi- and triserial endobenthic forms such as buliminids, which are considered particularly indicative of high food supply and low oxygenation (Jorissen et al., 2007; Corliss and Chen, 1988; Bernhard, 1986). This spike is therefore generally interpreted as a biological response to a short-lived period of anoxia following the K-Pg boundary impact (Speijer and Zwaan, 1996; Alegret et al., 2015). Likewise, at the upper bathyal Flaxbourne River section (New Zealand), the lowermost Paleocene, i.e. the sample directly above the 'fireball layer', is characterized by a benthic foraminiferal assemblage composed of small, inferred low-oxygen-tolerant taxa (Strong, 2000)

Also various lines of geochemical evidence have been postulated for the presence of short-lived hypoxia or anoxia on the shelfs following the K-Pg boundary. For example, the K-Pg boundary GSSP at El Kef is characterized by a spike in Total Organic Carbon (TOC) concentration, which was interpreted by (Keller and Lindinger, 1989) as representing low oxygen conditions at the sediment/water interface. Records form upper bathyal to neritic sites such as Caravaca (Spain), Hokkaido (Japan) and Stevns Klint (Denmark) show a sulfur isotopic excursion at the base of the boundary clay, which has been interpreted as bacterial

475 reduction of seawater sulfate, indicative of local anoxia (Kaiho et al., 1999; Kajiwara and
476 Kaiho, 1992; Schmitz et al., 1988).

477 Only few high-resolution K-Pg boundary redox-sensitive trace-elemental records
478 exist. The records of (Sosa-Montes De Oca et al., 2013) of the Caravaca section and
479 (Martinez-Ruiz et al., 1999) of the Agost section show an enrichment in typical redox-
480 sensitive elements like molybdenum and vanadium in the sample from the K-Pg boundary
481 ejecta layer. As this enrichment was only recorded within the boundary ejecta layer, the
482 authors argued that the oxygen depletion following the Chicxulub impact was very brief, in
483 the order of hundreds of years (Sosa-Montes De Oca et al., 2013).

484 Also ichnological analyses of the K-Pg boundary interval can provide insights in the
485 redox conditions across this interval (e.g. (Rodríguez-Tovar and Uchman, 2006, 2008), a
486 method that is particularly effective when combined with geochemical analyses of individual
487 trace fossils (Sosa-Montes de Oca et al., 2016). These methods have been extensively applied
488 on the Caravaca section (Rodríguez-Tovar and Uchman, 2006, 2008; Sosa-Montes de Oca et
489 al., 2016) and confirm that the anoxia/hypoxia following the K-Pg boundary impact was very
490 brief at this bathyal site.

491 Summarizing, various lines of evidence from widely separated shelf and bathyal sites
492 in Spain, France, Tunisia, Denmark, Japan, New Zealand, suggest short-lived hypoxia or
493 anoxia occurred directly following the Chicxulub impact. In upper bathyal sites such as
494 Caravaca and Bidart, these hypoxic/anoxic conditions appear to have been particularly short-
495 lived, i.e. limited to the first few hundred years following the impact (Sosa-Montes De Oca et
496 al., 2013). In some records, this phase was so short that it is only represented inside post-K-Pg
497 trace fossils hosted in uppermost Cretaceous strata (Alegret et al., 2015; Sosa-Montes de Oca
498 et al., 2016). Therefore, this signal is likely often missed in comparatively lower-resolution

studies (e.g. (Vellekoop et al., 2017). Evidence for hypoxic/anoxic conditions appears to be generally lacking from deeper marine K-Pg boundary sites (e.g. (Culver, 2003)), suggesting that this perturbation predominantly occurred at shallower marine sites. This observation is consistent with the hypothesis put forward in our study, that the recorded oxygen depletion resulted from decreased gas solubility and ocean ventilation resulting from the warming sea water, in combination with an increased oxygen demand in shelf bottom waters due to the increased nutrient inputs and resulting enhanced productivity.

REFERENCES

Alegret, L., Molina, E., and Thomas, E., 2003, Benthic foraminiferal turnover across the Cretaceous / Paleogene boundary at Agost (southeastern Spain): paleoenvironmental inferences: v. 48, doi: 10.1016/S0377-8398(03)00022-7.

Alegret, L., Rodr, F.J., and Uchman, A., 2015, How bioturbation obscured the Cretaceous–Palaeogene boundary record: Terra Nova, v. 27, p. 225–230, doi: 10.1111/ter.12151.

Alegret, L., and Thomas, E., 2009, Food supply to the sea floor in the Pacific Ocean after the Cretaceous/Paleogene boundary event: Marine Micropaleontology, v. 73, p. 105–116, doi: 10.1016/j.marmicro.2009.07.005.

Alvarez, L.W., Alvarez, W., Asaro, F., Michel, H. V, Alvarez, L.W., Alvarez, W., Asaro, F., and Michel, H. V, 1980, Extraterrestrial cause for the Cretaceous-Tertiary extinction: Science, v. 208, p. 1095–1108.

Anders, E., Wolbach, W.S., and Gilmour, I., 1990, Major wildfires at the Cretaceous-Tertiary boundary: Geological Society of America Special Papers, v. 247, p. 391–401, doi: 10.1130/SPE247-p391.

Artemieva, N., and Morgan, J., 2017, Quantifying the Release of Climate-Active Gases by Large Meteorite Impacts With a Case Study of Chicxulub: Geophysical Research Letters, v. 44, p. 1–9, doi: 10.1002/2017GL074879.

524 Asaro, F., Michel, H. V, Alvarez, W., Alvarez, L.W., Maddocks, R.F., and Bunch, T., 1982, Iridium and other
525 geochemical profiles near the Cretaceous-Tertiary boundary in a Brazos River section in Texas, *in*
526 Maddocks, R.F. ed., Texas ostracoda, International Symposium on Ostracoda, 8th, Guidebook of
527 Excursion and Related Papers, Univ. of Houston, Houston, p. 238–341.

528 Bauluz, B., Peacor, D.R., and Elliott, W.C., 2000, Coexisting altered glass and Fe-Ni oxides at the Cretaceous-
529 Tertiary boundary, Stevns Klint (Denmark): Direct evidence of meteorite impact: Earth and Planetary
530 Science Letters, v. 182, p. 127–136, doi: 10.1016/S0012-821X(00)00245-4.

531 Beerling, D.J., Lomax, B.H., Royer, D.L., Upchurch, G.R., and Kump, L.R., 2002, An atmospheric pCO2
532 reconstruction across the Cretaceous-Tertiary boundary from leaf megafossils: Proceedings of the National
533 Academy of Sciences of the United States of America, v. 99, p. 7836–7840.

534 Belcher, C.M., Finch, P., Collinson, M.E., Scott, A.C., and Grassineau, N. V, 2009, Geochemical evidence for
535 combustion of hydrocarbons during the K-T impact event:

536 Bernhard, J.M., 1986, Characteristic assemblages and morphologies of benthic foraminifera from anoxic,
537 organic-rich deposits; Jurassic through Holocene: Journal of Foraminiferal Research, v. 16, p. 207–215,
538 doi: 10.2113/gsjfr.16.3.207.

539 Bourgeois, J., Hansen, T.A., Wiberg, P.L., and Kauffman, E.G., 1988, A tsunami deposit at the Cretaceous-
540 Tertiary boundary in Texas: Science, v. 241, p. 567–570.

541 Brinkhuis, H., Bujak, J.P., Smit, J., Versteegh, G.J.M., and Visscher, H., 1998, Dinoflagellate-based sea surface
542 temperature reconstructions across the Cretaceous-Tertiary boundary: Palaeogeography,
543 Palaeoclimatology, Palaeoecology, v. 141, p. 67–83, doi: 10.1016/S0031-0182(98)00004-2.

544 Bromley, R.G., and Ekdale, A.A., 1987, Mass transport in European Cretaceous-chalk; fabric criteria for its
545 recognition: Sedimentology, v. 34, p. 1079–1092.

546 Brugger, J., Feulner, G., and Petri, S., 2016, Baby , it's cold outside: Climate model simulations of the effects of
547 the asteroid impact: Geophysical Research Letters, v. 44, p. 1–9, doi: doi:10.1002/2016GL072241.

548 Brumsack, H.J., 1980, Geochemistry of Cretaceous black shales from the Atlantic Pcean (DSDP Legs 11, 14, 36
549 and 41): Chemical Geology, v. 31, p. 1–25, doi: 10.1016/0009-2541(80)90064-9.

550 Coccioni, R., and Galeotti, S., 1994, K-T boundary extinction: Geologically instantaneous or gradual event ?
551 Evidence from deep-sea benthic foraminifera: Geology, v. 22, p. 779–782, doi: 10.1130/0091-
552 7613(1994)022<0779.

553 Corliss, B.H., and Chen, C., 1988, Morphotype patterns of Norwegian Sea deep-sea benthic foraminifera and
554 ecological implications: Geology, v. 16, p. 716–719, doi: 10.1130/0091-7613(1988)016<0716.

555 Culver, S.J.., 2003, Benthic foraminifera across the Cretaceous-Tertiary (K-T) boundary: a review: Marine
556 Micropaleontology, v. 47, p. 177–226.

557 Desor, E., 1847, Sur le terrain danien, nouvel étage de la craie: Bulletin de la Société Géologique de France, v. 4,
558 p. 179–182.

559 Emerson, S.R., and Huested, S.S., 1991, Ocean anoxia and the concentrations of molybdenum and vanadium in
560 seawater: Marine Chemistry, v. 34, p. 177–196, doi: 10.1016/0304-4203(91)90002-E.

561 Eshet, Y., Almogi-Labin, A., and Bein, A., 1994, Dinoflagellate cysts, paleoproductivity and upwelling systems:
562 A Late Cretaceous example from Israel: Marine Micropaleontology, v. 23, p. 231–240, doi: 10.1016/0377-
563 8398(94)90014-0.

564 FitzPatrick, M.E.J., Forber, D.A., and Hart, M.B., 2017, Dinocyst stratigraphy and palaeoenvironmental
565 interpretation of the Cretaceous/Paleogene boundary at Stevns Klint, Denmark: Cretaceous Research, doi:
566 10.1016/j.cretres.2017.09.001.

567 Galeotti, S., Brinkhuis, H., and Huber, M., 2004, Records of post-Cretaceous-Tertiary boundary millennial-scale
568 cooling from the western Tethys: A smoking gun for the impact-winter hypothesis? Geology, v. 32, p.
569 529–532, doi: 10.1130/G20439.1.

570 Ganapathy, R., Gartner, R., and Jiang, M.-J., 1981, Iridium anomaly at the Cretaceous-Tertiary boundary in
571 Texas: Earth and Planetary Science Letters, v. 54, p. 393–396.

572 Gardin, S., 2002, Late Maastrichtian to early Danian calcareous nannofossils at Elles (Northwest Tunisia). A tale
573 of one million years across the K-T boundary: Palaeogeography, Palaeoclimatology, Palaeoecology, v.
574 178, p. 211–231, doi: 10.1016/S0031-0182(01)00397-2.

575 Hansen, J.M., 1977, Dinoflagellate stratigraphy and echinoid distribution in Upper Maastrichtian and Danian

deposits from Denmark: Bulletin of the Geological Society of Denmark, v. 26, p. 1–26.

Hansen, T., Farrand, R.B., Montgomery, H.A., and Blechschmidt, G., 1987, Sedimentology and extinction patterns across the Cretaceous-Tertiary boundary interval in East Texas: Cretaceous Research, v. 8, p. 229–252.

Hansen, T., and Surlyk, F., 2014, Marine macrofossil communities in the uppermost Maastrichtian chalk of Stevns Klint, Denmark: Palaeogeography, Palaeoclimatology, Palaeoecology, v. 399, p. 323–344, doi: 10.1016/j.palaeo.2014.01.025.

Hansen, T.A., Upshaw III, B., Kauffman, E.G., and Gose, W., 1993, Patterns of molluscan extinction and recovery across the Cretaceous–Tertiary boundary in east Texas: report on new outcrops.: Cretaceous Research, v. 14, p. 685–706.

Hart, M.B., Feist, S.E., Hakansson, E., Heinberg, C., Price, G.D., Leng, M.J., and Watkinson, M.P., 2005, The Cretaceous-Palaeogene boundary succession at Stevns Klint, Denmark: Foraminifers and stable isotope stratigraphy: Palaeogeography, Palaeoclimatology, Palaeoecology, v. 224, p. 6–26, doi: 10.1016/j.palaeo.2005.03.029.

Hart, M.B., Feist, S.E., Price, G.D., and Leng, M.J., 2004, Reappraisal of the K-T boundary succession at Stevns Klint, Denmark: Journal of the Geological Society, v. 161, p. 885–892, doi: 10.1144/0016-764903-071.

Hart, M.B., Yancey, T.E., Leighton, A.D., Miller, B., Liu, C., Smart, C.W., and Twitchett, R.J., 2012, The Cretaceous-Paleogene boundary on the Brazos River, Texas: New stratigraphic sections and revised interpretations: GCAGS Journal, v. 1, p. 69–80.

Harvey, M.C., Brassell, S.C., Belcher, C.M., and Montanari, A., 2008, Combustion of fossil organic matter at the Cretaceous-Paleogene (K-P) boundary: Geology, v. 36, p. 355–358, doi: 10.1130/G24646A.1.

Helz, G.R., Miller, C. V., Charnock, J.M., Mosselmans, J.F.W., Pattrick, R.A.D., Garner, C.D., and Vaughan, D.J., 1996, Mechanism of molybdenum removal from the sea and its concentration in black shales: EXAFS evidence: Geochimica et Cosmochimica Acta, v. 60, p. 3631–3642, doi: 10.1016/0016-7037(96)00195-0.

Heymann, D., Yancey, T.E., Wolbach, W.S., Thiemens, M.H., Johnson, E.A., Roach, D., and Moecker, S., 1998, Geochemical markers of the Cretaceous-Tertiary boundary event at Brazos River, Texas, USA:

603 Geochimica et Cosmochimica Acta, v. 62, p. 173–181.

604 Hildebrand, A.R., Penfield, G.T., Kring, D.A., Pilkington, M., Carmago Z., A., Jacobsen, S.B., and Boyton, W.
605 V, 1991, Chicxulub Crater: A possible Cretaceous/Tertiary boundary impact crater on the Yucatán
606 Peninsula, Mexico: Geology, v. 19, p. 867–871.

607 Hilting, A.K., Kump, L.R., and Bralower, T.J., 2008, Variations in the oceanic vertical carbon isotope gradient
608 and their implications for the Paleocene-Eocene biological pump: Paleoceanography, v. 23, p. 1–15, doi:
609 10.1029/2007PA001458.

610 Hondt, S.D., 2005, Consequences of the Cretaceous/Paleogene mass extinction for marine ecosystems: Annual
611 Review of Ecological and Evolutionary Systems, v. 36, p. 295–317, doi:
612 10.1146/annurev.ecolsys.35.021103.105715.

613 Hunter, S.J., Valdes, P.J., Haywood, A.M., and Markwick, P.J., 2008, Modelling Maastrichtian climate:
614 investigating the role of geography , atmospheric CO 2 and vegetation: Climate of the Past Discussions, v.
615 4, p. 981–1019.

616 Ivanov, B.A., Badukov, D.D., Yakovlev, O.I., Gerasimov, M. V, Dikov, Y.P., Pope, K.O., and Ocampo, A.C.,
617 1996, Degassing of sedimentary rocks due to Chicxulub impact: Hydrocode and physical simulations:
618 Geological Society of America Special Paper, v. 307, p. 125–140.

619 Ivanov, B. a, and Deutsch, A., 2002, The phase diagram of CaCO3 in relation to shock compression and
620 decomposition: Physics of the Earth and Planetary Interiors, v. 129, p. 131–143, doi: 10.1016/S0031-
621 9201(01)00268-0.

622 Jiang, M.J., and Gartner, S., 1986, Calcareous nannofossil succession across the Cretaceous/Tertiary boundary in
623 east-central Texas.: Micropaleontology, v. 32, p. 232–255.

624 Jorissen, F.J., Fontanier, C., and Thomas, E., 2007, Paleoceanographical proxies based on deep-sea benthic
625 foraminiferal assemblage characteristics, *in* Hillaire-Marcel, C. and de Vernal, A. eds., Proxies in Late
626 Cenozoic Paleoceanography: Pt. 2, Elsevier, p. 263–326, doi: 10.1016/S1572-5480(07)01012-3.

627 Jorissen, F.J., de Stigter, H.C., and Widmark, J.G. V, 1995, A conceptual model explaining benthic foraminiferal
628 microhabitats: Marine Micropaleontology, v. 26, p. 3–15.

629 Kaiho, K., 1994, Benthic foraminiferal dissolved-oxygen index and dissolved-oxygen levels in the modern
630 ocean: Geology, v. 22, p. 719–722.

631 Kaiho, K., Kajiwara, Y., Tazaki, K., Ueshima, M., Takeda, N., Kawahata, H., Arinobu, T., Ishiwatari, R., Hirai,
632 A., and Lamolda, M.A., 1999, Oceanic primary productivity and dissolved oxygen levels at the
633 Cretaceous/Tertiary boundary: Their decrease, subsequent warming, and recovery: Paleoceanography, v.
634 14, p. 511–524, doi: 10.1029/1999PA900022.

635 Kaiho, K., and Oshima, N., 2017, Site of asteroid impact changed the history of life on Earth: the low probability
636 of mass extinction: Scientific Reports, v. 7, p. 14855, doi: 10.1038/s41598-017-14199-x.

637 Kajiwara, Y., and Kaiho, K., 1992, Oceanic anoxia at the cretaceous/tertiary boundary supported by the sulfur
638 isotopic record: Palaeogeography, Palaeoclimatology, Palaeoecology, doi: 10.1016/0031-0182(92)90012-
639 T.

640 Kawaragi, K., Sekine, Y., Kadono, T., Sugita, S., Ohno, S., Ishibashi, K., Kurosawa, K., Matsui, T., and Ikeda,
641 S., 2009, Direct measurements of chemical composition of shock-induced gases from calcite : an intense
642 global warming after the Chicxulub impact due to the indirect greenhouse effect of carbon monoxide:
643 Earth and Planetary Science Letters, v. 282, p. 56–64, doi: 10.1016/j.epsl.2009.02.037.

644 Keller, G., and Lindinger, M., 1989, Stable isotope, TOC and CaCO3 record across the Cretaceous/ Tertiary
645 boundary at El Kef, Tunisia: Palaeogeography, Palaeoclimatology, Palaeoecology, v. 73, p. 243–265.

646 Kennedy, W.J., Landman, N.H., Christensen, W.K., Cobban, W. a, and Hancock, J.M., 1998, Marine
647 connections in North America during the late Maastrichtian: Palaeogeographic and palaeobiogeographic
648 significance of Jeletzkytes nebrascensis Zone cephalopod fauna from the Elk Butte Member of the Pierre
649 Shale, SE South Dakota and NE Nebraska: Cretaceous Research, v. 19, p. 745–775, doi:
650 10.1006/cres.1998.0129.

651 Korchagin, O.A., and Tsel'movich, V.A., 2011, Cosmic particles (micrometeorites) and nanospheres from the
652 Cretaceous-Paleogene (K/T) boundary clay layer at the Stevns Klint Section, Denmark: Doklady Earth
653 Sciences, v. 437, p. 449–454, doi: 10.1134/s1028334x11040039.

654 Kring, D.A., and Durda, D.D., 2002, Trajectories and distribution of material ejected from the Chicxulub impact
655 crater: Implications for postimpact wildfires: Journal of Geophysical Research: Planets, v. 107, p. 6–1–6–

22, doi: 10.1029/2001JE001532.

Lottaroli, F., and Catrullo, D., 2000, The calcareous nannofossil biostratigraphic framework of the Late Maastrichtian-Danian North Sea chalk: Marine Micropaleontology, v. 39, p. 239–263, doi: 10.1016/S0377-8398(00)00023-2.

Martinez-Ruiz, F., Ortega-Huertas, M., and Palomo, I., 1999, Positive Eu anomaly development during diagenesis of the K/T boundary ejecta layer in the Agosta section (SE Spain): Implications for trace-element remobilization: Terra Nova, v. 11, p. 290–296, doi: 10.1046/j.1365-3121.1999.00261.x.

Martinez-Ruiz, F., Ortega-Huertas, M., and Rivas, P., 2006, Rare earth element composition as evidence of the precursor material of Cretaceous-Tertiary boundary sediments at distal sections: Chemical Geology, v. 232, p. 1–11, doi: 10.1016/j.chemgeo.2006.02.013.

Molina, E., Alegret, L., Arenillas, I., Arz, J.A., Gallala, N., Hardenbol, J., von Salis, K., Steurbaut, E., Vandenberghe, N., and Zaghbib-Turki, D., 2006, The Global Boundary Stratotype Section and Point for the base of the Danian Stage (Paleocene, Paleogene," Tertiary", Cenozoic) at El Kef, Tunisia-Original definition and revision: Episodes, v. 29, p. 263–273.

O'Keefe, J.D., and Ahrens, T.J., 1989, Impact production of CO2 by the Cretaceous/Tertiary extinction bolide and the resultant heating of the Earth: Nature, v. 338, p. 247–249.

Olsson, R.K., Hemleben, C., Berggren, W.A., and Huber, B.T., 1999, Atlas of Paleocene Planktonic Foraminifera: Smithsonian Contributions to Paleobiology, v. 85, p. 1–252, doi: 10.5479/si.00810266.85.1.

Pierazzo, E., Kring, D.A., and Melosh, H.J., 1998, Hydrocode simulation of the Chicxulub impact event and the production of climatically active gases: Journal of Geophysical Research, v. 103, p. 28607, doi: 10.1029/98JE02496.

Pope, K.O., Baines, K.H., Ocampo, A.C., and Ivanov, B.A., 1997, Energy, volitile production, and climatic effects of the Chicxulub Cretaceous/Tertiary impact: Journal of Geophysical Research, v. 102, p. 21645–21664.

Potter, C.S., Klooster, S.A., and Ames, N., 1999, Dynamic global vegetation modelling for prediction of plant functional types and biogenic trace gas fluxes: Global Ecology and Biogeography, v. 8, p. 473–488.

682 Premovic, P.I., 2009, The conspicuous red “impact” layer of the Fish Clay at Højerup (Stevns Klint, Denmark):
683 Geochemistry International, v. 47, p. 513–521.

684 Rasmussen, J.A., Heinberg, C., and Håkansson, E., 2005, Planktonic foraminifers, biostratigraphy and the
685 diachronous nature of the lowermost Danian Cerithium Limestone at Stevns Klint, Denmark: Bulletin of
686 the Geological Society of Denmark, v. 52, p. 113–131.

687 Robin, E., Boclet, D., Bonté, P., Froget, L., Jéhanno, C., and Rocchia, R., 1991, The stratigraphic distribution of
688 Ni-rich spinels in Cretaceous-Tertiary boundary rocks at El Kef (Tunisia), Caravaca (Spain) and Hole
689 761C (Leg 122): Earth and Planetary Science Letters, v. 107, p. 715–721, doi: 10.1016/0012-
690 821X(91)90113-V.

691 Rocchia, R., Robin, E., Froget, L., and Gayraud, J., 1996, Stratigraphic distribution of extraterrestrial markers at
692 the Cretaceous-Tertiary boundary in the Gulf of Mexico area: implications for the temporal complexity of
693 the event.: Geological Society of America Special Paper, v. 307, p. 279–286.

694 Rodríguez-Tovar, F.J., and Uchman, A., 2008, Bioturbational disturbance of the Cretaceous-Palaeogene (K-Pg)
695 boundary layer: Implications for the interpretation of the K-Pg boundary impact event: Geobios, v. 41, p.
696 661–667, doi: 10.1016/j.geobios.2008.01.003.

697 Rodríguez-Tovar, F.J., and Uchman, A., 2006, Ichnological analysis of the Cretaceous-Palaeogene boundary
698 interval at the Caravaca section, SE Spain: Palaeogeography, Palaeoclimatology, Palaeoecology, v. 242, p.
699 313–325, doi: 10.1016/j.palaeo.2006.06.006.

700 Royer, D.L., Pagani, M., Beerling, D.J., Haven, N., and Sciences, P., 2012, Geobiological constraints on Earth
701 system sensitivity to CO2 during the Cretaceous and Cenozoic: Geobiology, v. 10, p. 298–310, doi:
702 10.1111/j.1472-4669.2012.00320.x.

703 Sarmiento, J.L., Dunne, J.P., and Armstrong, R.A., 2004, Do we now understand the ocean’s biological pump?,:
704 U.S. Joint Global Ocean Flux Study News, v. 12, p. 1–5.

705 Schmitz, B., Andersson, P., and Dahl, J., 1988, Iridium, sulfur isotopes and rare earth elements in the
706 Cretaceous-Tertiary boundary clay at Stevns Klint, Denmark: Geochimica et Cosmochimica Acta, v. 52, p.
707 229–236, doi: 10.1016/0016-7037(88)90072-5.

708 Schmitz, B., Keller, G., and Stenvall, O., 1992, Stable isotope and foraminiferal changes across the Cretaceous-

709 Tertiary boundary at Stevns Klint, Denmark: Arguments for long-term oceanic instability before and after
710 bolide-impact event: Palaeogeography, Palaeoclimatology, Palaeoecology, v. 96, p. 233–260.

711 Scotese, C.R., and Dreher, C., 2012, GlobalGeology:, http:/www.GlobalGeology.com.

712 Scott, C., and Lyons, T.W., 2012, Contrasting molybdenum cycling and isotopic properties in euxinic versus
713 non-euxinic sediments and sedimentary rocks: Refining the paleoproxies: Chemical Geology, v. 324–325,
714 p. 19–27, doi: 10.1016/j.chemgeo.2012.05.012.

715 Sluijs, A., and Brinkhuis, H., 2009, A dynamic climate and ecosystem state during the Paleocene-Eocene
716 Thermal Maximum – inferences from dinoflagellate cyst assemblages at the New Jersey Shelf:
717 Biogeosciences, v. 6, p. 5163–5215, doi: 10.5194/bgd-6-5163-2009.

718 Smit, J., 1977, Discovery of a planktonic foraminiferal association between the Abathomphalus mayaroensis
719 zone and the “Globigerina” eugubina zone at the Cretaceous/Tertiary boundary in the Barranco del
720 Gredero (Caravaca, SE Spain): a preliminary report.: Proc. Koninklijke Nederlandse Akademie van
721 Wetenschappen, v. 80, p. 280–301.

722 Smit, J., 1982, Extinction and evolution of planktonic foraminifera after a major impact at the
723 Cretaceous/Tertiary boundary: Geological Society of America Special Paper, v. 190, p. 329–252.

724 Smit, J., 1990, Meteorite impact, extinctions and the Cretaceous-Tertiary boundary: Geologie en Mijnbouw, v.
725 69, p. 187–204.

726 Smit, J., 2004, The section of the Barranco del Gredero (Caravaca , SE Spain): a crucial section for the
727 Cretaceous / Tertiary boundary impact extinction hypothesis: Journal of Iberian Geology, v. 31, p. 179–
728 191.

729 Smit, J., Roep, T.B., Alvarez, W., Montanari, A., Claeys, P., Grajales-Nishimura, J.M., and Bermudez, J., 1996,
730 Coarse-grained, clastic sandstone complex at the K/T boundary around the Gulf of Mexico: Deposition by
731 tsunami waves induced by the Chicxulub impact? Geological Society of America Special Papers, v. 307, p.
732 151–182, doi: 10.1130/0-8137-2307-8.151.

733 Sosa-Montes De Oca, C., Martínez-Ruiz, F., and Rodríguez-Tovar, F.J., 2013, Bottom-water conditions in a
734 marine basin after the cretaceous-paleogene impact event: Timing the recovery of oxygen levels and
735 productivity: PLoS ONE, v. 8, p. 1–7, doi: 10.1371/journal.pone.0082242.

736 Sosa-Montes de Oca, C., Rodríguez-Tovar, F.J., and Martínez-Ruiz, F., 2016, Geochemical and isotopic
737 characterization of trace fossil infillings: New insights on tracemaker activity after the K/Pg impact event:
738 Cretaceous Research, v. 57, p. 391–401, doi: 10.1016/j.cretres.2015.03.003.

739 Speijer, R.P., and Zwaan, G.J. Van Der, 1996, Extinction and survivorship of southern Tethyan Benthic
740 foraminifera across the Cretaceous/Palaeogene boundary, *in* Hart, M.B. ed., Biotic Recovery from Mass
741 Extinction Events, London, Geological Society Special Publication, v. 102, p. 343–371, doi:
742 10.1144/GSL.SP.1996.001.01.26.

743 Strong, C.P., 2000, Cretaceous-Tertiary foraminiferal succession at Flaxbourne River, Marlborough, New
744 Zealand: New Zealand Journal of Geology and Geophysics, v. 43, p. 1–20, doi:
745 10.1080/00288306.2000.9514867.

746 Surlyk, F., Damholt, T., and Bjerager, M., 2006, Stevns Klint, Denmark: Uppermost Maastrichtian chalk,
747 Cretaceous-Tertiary boundary, and lower Danian bryozoan mound complex: Bulletin of the Geological
748 Society of Denmark, v. 54, p. 1–48.

749 Takata, T., and Ahrens, T.J., 1994, Numerical simulation of impact cratering at Chicxulub and the possible
750 causes of KT catastrophe, *in* New Developments Regarding the KT Event and Other Catastrophes in Earth
751 History, Houston, the Lunar and Planetary Institute, p. 125–126.

752 Thomson, J., Higgs, N.C., Wilson, T.R.S., Croudace, I.W., De Lange, G.J., and Van Santvoort, P.J.M., 1995,
753 Redistribution and geochemical behaviour of redox-sensitive elements around S1, the most recent eastern
754 Mediterranean sapropel: Geochimica et Cosmochimica Acta, v. 59, p. 3487–3501, doi: 10.1016/0016-
755 7037(95)00232-O.

756 Vajda, V., and Bercovici, A., 2014, The global vegetation pattern across the Cretaceous-Paleogene mass
757 extinction interval: A template for other extinction events: Global and Planetary Change, v. 122, p. 29–49,
758 doi: 10.1016/j.gloplacha.2014.07.014.

759 Vajda, V., Raine, J.I., and Hollis, C.J., 2001, Indication of Global Deforestation at the Cretaceous-Tertiary
760 Boundary by New Zealand Fern Spike: Science, v. 294, p. 1700–1702.

761 Vandenberghe, N., Hilgen, F.J., Speijer, R.P., Ogg, J.G., Gradstein, F.M., Hammer, Ø., Hollis, C.J., and Hooker,
762 J.J., 2012, The Paleogene Period: Elsevier, v. 1–2, 855-921 p., doi: 10.1016/B978-0-444-59425-9.00028-7.

763 Vellekoop, J., Sluijs, A., Smit, J., Schouten, S., Weijers, J.W.H., Sinninghe Damsté, J.S., and Brinkhuis, H.,
764 2014, Rapid short-term cooling following the Chicxulub impact at the Cretaceous-Paleogene boundary.:
765 Proceedings of the National Academy of Sciences of the United States of America, v. 111, p. 1–5, doi:
766 10.1073/pnas.1319253111.

767 Vellekoop, J., Woelders, L., Açikalin, S., Smit, J., van de Schootbrugge, B., Yilmaz, I.O., Brinkhuis, H., and
768 Speijer, R.P., 2017, Ecological response to collapse of the biological pump following the mass extinction
769 at the Cretaceous-Paleogene boundary: Biogeosciences, v. 14, p. 885–900, doi: doi:10.5194/bg-14-885-
770 2017.

771 Venkatesan, M.I., and Dahl, J., 1989, Organic geochemical evidence for global fires at the Cretaceous/Tertiary
772 boundary: Nature, v. 338, p. 57–60.

773 Wade, B.S., Pearson, P.N., Berggren, W.A., and Pälike, H., 2011, Review and revision of Cenozoic tropical
774 planktonic foraminiferal biostratigraphy and calibration to the geomagnetic polarity and astronomical time
775 scale: Earth-Science Reviews, v. 104, p. 111–142, doi: 10.1016/j.earscirev.2010.09.003.

776 Woelders, L., and Speijer, R.P., 2015, Stable seafloor conditions, sea level and food supply during the latest
777 Maastrichtian at Brazos River, Texas: Marine Micropaleontology, v. 121, p. 41–51, doi:
778 10.1016/j.marmicro.2015.10.002.

779 Yancey, T.E., 1996, Stratigraphy and depositional environments of the Cretaceous-Tertiary boundary complex
780 and basal Paleocene section, Brazos River, Texas: Transactions of the Gulf Coast Association of
781 Geological Societies, v. 46, p. 433–442.

782

783

784

785

786

787

788

789

790

SI FIGURES

SI Figure S1

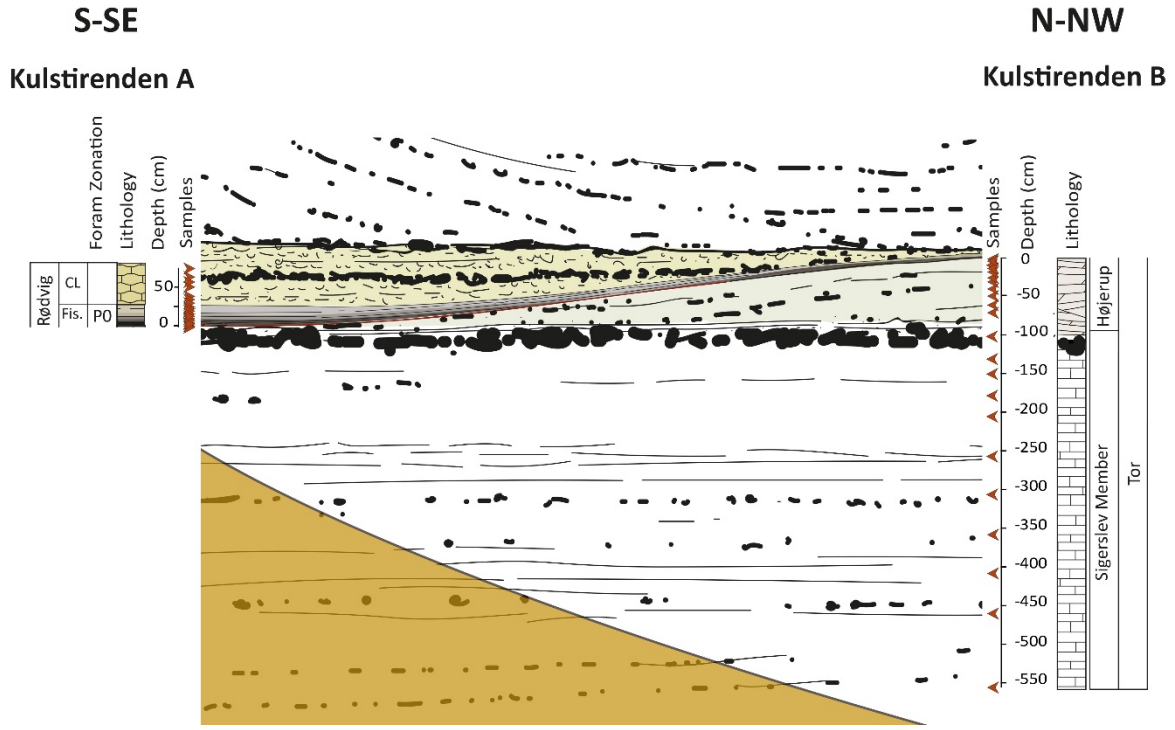

SI Figure S1 caption

The two sample localities at Kulstirenden, Stevns Klint, Denmark. To allow for relative high temporal resolution in both the topmost Cretaceous and basal Paleogene, the Fiskeler Member was sampled in one of the basins between the Hojerup Member bryozoan mound crests, where the Fiskeler K-Pg boundary clay reaches a thickness of 27-28 cm (Kulstirenden A), while the Sigerslev and Hojerup members were sampled about 15 meters laterally from this point, where the Hojerup Member reaches a thickness of approximately 1 meter (Kulstirenden B). Consequently, the Kulstirenden record used in this study is a composite (splice) record. The lower part of the sequence at Kulstirenden A is covered by overburden. This schematic drawing has a vertical exaggeration of 2x.

SI Figure S2

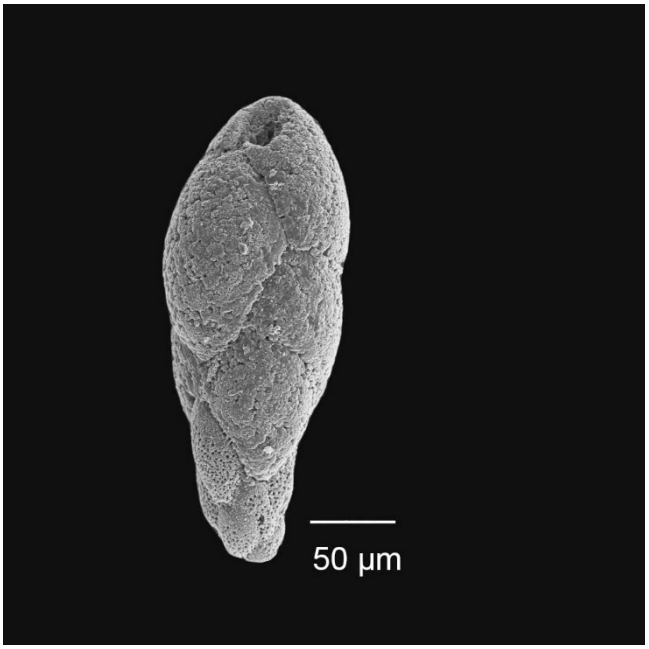

SI Figure S2 caption

Fursenkoina sp. (Loeblich and Tappan). Brazos-1 sample BR4a (18.5 cm above base limestone).

SI Figure S3

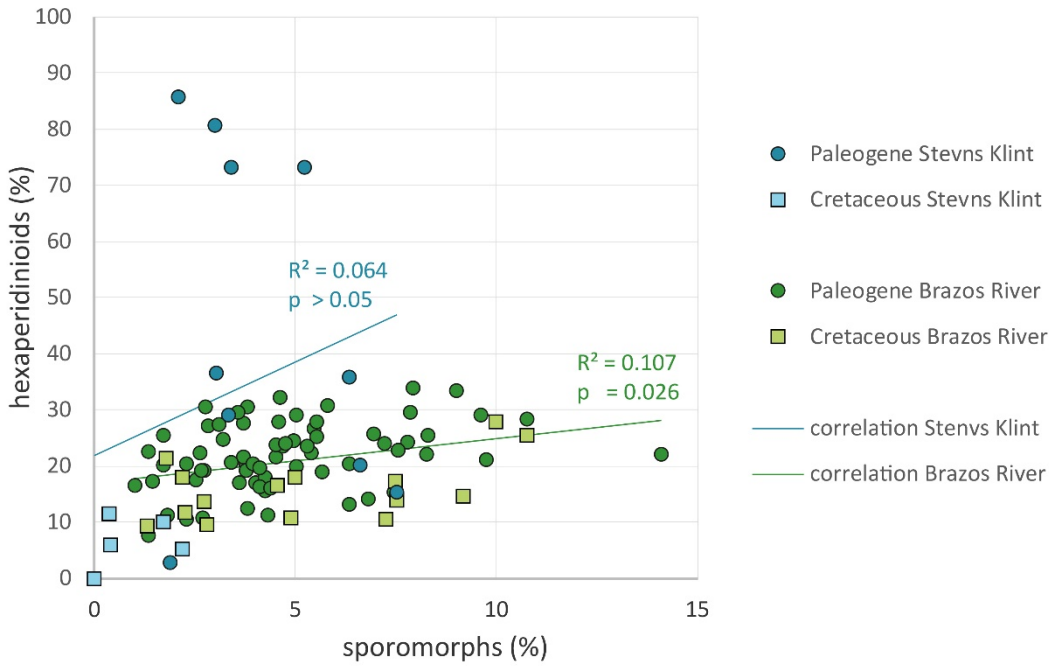

SI Figure S3 caption

Relative abundances of hexaperidinioids against the relative abundances of sporomorphs for the Brazos -1 and Stevns Klint composite sections, indicating that there is a weak but statistically significant correlation between the relative abundances of hexaperidinoids and relative abundances of sporomorphs at Brazos-1, but no statistically significant correlation between these parameters at Stevns Klint.

822 SI Figure S4

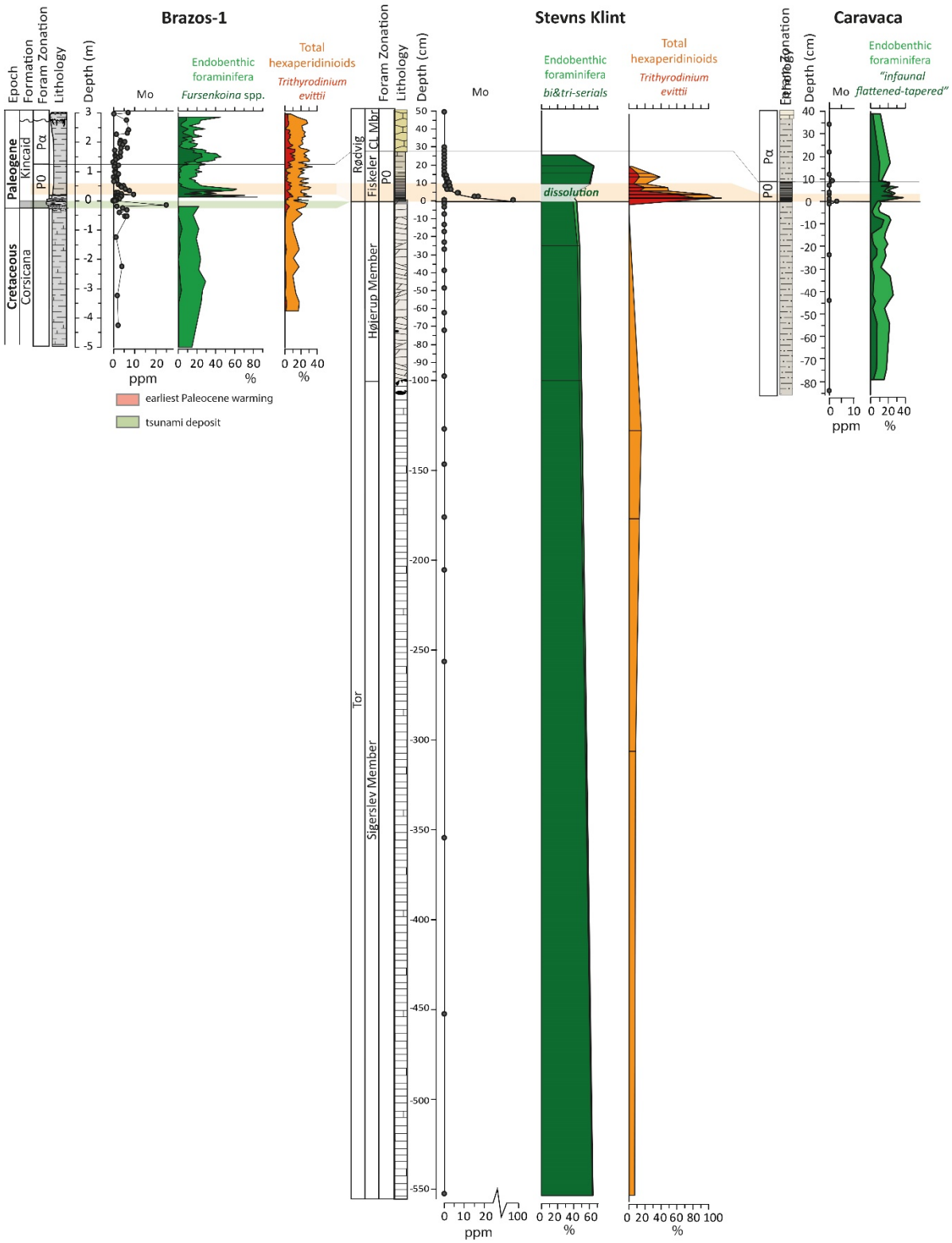

823

824

SI Figure S4 caption

Mo, benthic foraminiferal and palynological records of Brazos-1, the Stevns Klint composite and Caravaca. The earliest Paleocene warming is indicated in red. The benthic foraminiferal record of Caravaca is from (Coccioni and Galeotti, 1994). The lower 10 cm of the Paleocene of Stevns Klint is characterized by strong dissolution.

SI TABLES

SI Table S1 caption

major and minor element compositions Brazos -1, Stevns Klint and Caravaca sections.

SI Table S2 caption

Benthic foraminiferal data of the Brazos -1 and Stevns Klint sections.

SI Table S3 caption

Marine palynological data of the Brazos -1 and Stevns Klint sections.